RSC Advances

PAPER

View Article Online
View Journal | View Issue

Cite this: *RSC Adv.*, 2015, **5**, 102803

Photovoltaic performance of a N719 dye based dye-sensitized solar cell with transparent macroporous anti-ultraviolet photonic crystal coatings

Chang-Yun Cai,[a] Sheng-Kai Tseng,[a] Meng Kuo,[a] Kun-Yi Andrew Lin,[b] Hongta Yang*[a] and Rong-Ho Lee*[a]

Received 13th October 2015
Accepted 24th November 2015

DOI: 10.1039/c5ra21194h

www.rsc.org/advances

This article reports a scalable and roll-to-roll compatible bottom-up self-assembly technology for fabricating macroporous photonic crystal-based polymer films on the reverse side of a photoanode deposited substrate of a dye-sensitized solar cell (DSSC). Both optical measurements and theoretical predications revealed that the as-prepared transparent macroporous films consisting of three-dimensional ordered 200 nm air cavities exhibited anti-ultraviolet (anti-UV) property caused by the Bragg diffraction of ultraviolet radiation from the crystalline lattice of air cavities in the polymer films. The UV-shielding effects on the electrochemical impedance properties and photovoltaic (PV) performance of the UV light illuminated DSSC were studied. The PV properties of the DSSC without the UV-shielding film were decreased significantly as compared to that of the DSSC with the UV-shielding film. The efficiency decay of DSSCs was greatly alleviated by the UV-shielding of such a macroporous polymer film.

1. Introduction

In recent years, there has been growing interest in developing dye-sensitized solar cells (DSSCs) due to the low cost and flexibility of materials.[1,2] A DSSC consists of a titanium oxide (TiO_2) layer based photo-electrode, adsorbed photosensitive dye, aniodide/triiodine redox couple in a solvent as an electrolyte, and a Pt-coated counter electrode. As the photosensitive dye absorbs solar radiation, dye molecules in the photo-excited state inject electrons and holes into the TiO_2 and electrolyte, respectively. Electrons can then transport through the TiO_2 and holes through the electrolyte to their respective electrodes, where they are collected in an external circuit. The solar energy conversion efficiencies of DSSCs featuring liquid electrolytes can even reach approximately 11%.[3,4]

In addition to the photo-energy conversion efficiency (PCE), the operational stability is another important issue to be addressed in practical solar energy applications.[5,6] The degradation of sensitized dye and electrolyte of DSSC have been systemically investigated.[6–12] Among the degradation mechanisms, it is reported that the absorption intensity of the CN stretching band from the thiocyanate ion ligand of ruthenium dye N719 decreased under UV irradiation.[7] Additionally, the iodine in electrolyte also degrades by UV irradiation, leading to a bleaching of electrolyte solution.[9,13] The ion exchange between the thiocyanate ion ligand and the redox couple iodide/triiodide (I^-/I_3^-) in electrolyte solution causes the degradation of N719 dye.[7] Moreover, it is reported that the redox couple I^-/I_3^- containing yellow electrolyte solution results in a chromatization in DSSC under UV irradiation[14] Therefore, solar sensitized dyes and electrolytes are vulnerable to UV radiation through the photochemical reaction.[8,15,16]

To eliminate the challenges, it is desirable to develop UV-shielding materials suitable for DSSCs. Numbers of studies have recently reported on the preparation of UV-shielding materials *via* structural design of polymer molecules,[17,18] addition of organic UV radiation absorbents,[19,20] or introduction of nanoparticles to polymeric matrix.[21,22] Unfortunately, the current techniques are relatively difficult and costly. Photonic crystals, exemplified by Blue Morpho butterfly wing scales, provide a platform for investigating diffractive optical switches and filters.[23] A large variety of colloidal self-assembly methodologies have been utilized for creating highly order colloidal crystals.[24–31] However, most of the current self-assembly technologies are only favorable for low-volume, laboratory-scale production. To resolve the scale-up and cost issues, a simple and roll-to-roll compatible doctor blade coatings (DBC) technology that enables the fabrication of self-standing three-dimensional highly ordered macroporous membranes is proposed in this study and used as anti-UV coatings for application in DSSCs. In order to demonstrate the UV-shielding

[a]*Department of Chemical Engineering, National Chung Hsing University, 250 Kuo-Kuang Road, Taichung 40227, Taiwan. E-mail: hyang@dragon.nchu.edu.tw; rhl@dragon.nchu.edu.tw; Fax: +886-4-22854734; Tel: +886-4-22854724; +886-4-22854308*

[b]*Department of Environmental Engineering, National Chung Hsing University, 250 Kuo-Kuang Road, Taichung 40227, Taiwan*

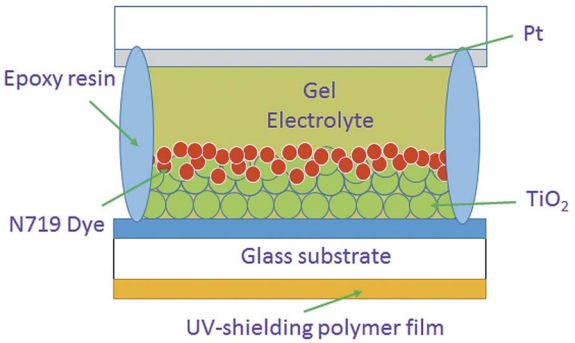

Fig. 1 Architecture of DSSC with UV-shielding polymer film.

performance on the organic sensitized dye and electrolyte in DSSC, macroporous photonic crystal based UV-shielding polymer film was doctor blade coated on the reverse side of the fluorine-doped tin oxide (FTO) coated glass substrates. The macroporous film coated FTO glass was then used as an anode to fabricate N719 dye based DSSCs (Fig. 1). The UV light damage effects on the PV properties of the DSSCs with and without the UV protecting film were studied.

2. Experimental

2.1 Preparation of UV-shielding polymer film

In this study, monodispersed silica microspheres with diameter of 200 nm were synthesized by the well-established Stöber method.[32] The as-synthesized silica microspheres were purified in dehydrated ethanol by multiple centrifugation/redispersion cycles to remove impurities, followed by redispersing in ethoxylated trimethylolpropane triacrylate monomer (ETPTA, SR454) with 1 vol% 2-hydroxy-2-methyl-1-phenyl-1-propanone (Darocur 1173) as a photo-initiator. The silica microsphere volume fraction of the colloidal suspension was adjusted to be 74 vol%. After filtration through a 5 μm syringe filter to remove particle aggregates, the viscous and transparent solution was collected. As shown in Fig. 2, an immobilized doctor blade was placed on an ETPTA wetting layer coated glass. The as-prepared suspension was dispensed along one sidewall of the blade onto the substrate. The substrate was then dragged at a controlled rate of 1 mm min^{-1} by a syringe pump (KD Scientific 780-230). In the coating process, the doctor blade was introduced for applying a one-dimensional shear force to align colloidal particles. The ETPTA monomer was finally photo-polymerized by exposure to UV radiation to obtain a silica colloidal crystal–polymer composite. The composite was then immersed in a 1 vol% hydrofluoric acid aqueous solution to selectively remove the templating silica particles, followed by washing in 200 proof ethanol and drying in a steam of nitrogen. These procedures were repeated for multiple cycles to collect macroporous polymer film.

2.2 Fabrication of DSSCs

To measure PV properties, DSSCs having an active area of 0.25 cm^2 were fabricated.[11] The FTO conducting glass (FTO; sheet resistance: 15 Ω sq^{-1}; Solaronix) with UV-shielding polymer film on the reverse side of the glass substrate was used as the electrode of DSSC. A TiO_2 thin film electrode was prepared as follows: TiO_2 (1 g) was mixed with poly-oxyethylene (10) octylphenyl ether (Triton X-100, 0.4 mL) and 5 wt% aqueous acetic acid (5 mL) and ground mechanically. The obtained TiO_2 paste was coated on surface of FTO based electrode using the doctor blade method.[33] After coating, the thin film electrode was dried at room temperature and then sintered at 500 °C for 2 h. The resulting film was used as the photo-electrode of DSSC. The thickness of the TiO_2 layer was about 10 μm. The surface of the calcined TiO_2 electrode was soaked in 0.5 mM ruthenium dye (N719 dye, Solaronix) in acetonitrile (MeCN)/*tert*-butanol (1 : 1, v/v).[33] The counter electrodes were Pt-coated indium tin oxide (ITO) glass. The gel electrolyte was prepared by mixing LiI (0.068 g), I_2 (0.064 g), 4-*t*-butylpyridine (TBP, 0.4 mL), 1-propyl-2,3-dimethylimidazolium iodide (PMII, 0.8 g), and polyethylene oxide (0.44 g, Mn = 300 000 g mol^{-1}) with propylene carbonate (4.6 mL). Finally, the N719 dye-adsorbed photoelectrode and counter electrode were placed side by side and the gel electrolyte was poured into the space between them. The cell was sealed with thermal-cured epoxy glue. After encapsulation, the DSSC sample was obtained.

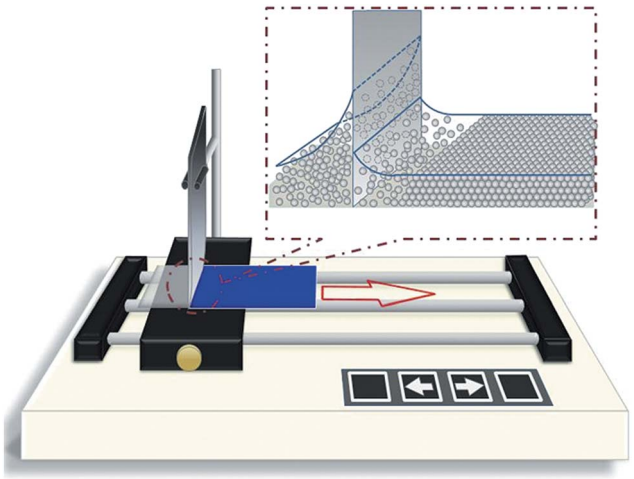

Fig. 2 Schematic illustration of the experimental setup for fabricating colloidal crystal–polymer composites by using a doctor blade coating technique.

2.3 Characterization of DSSCs

Fourier transform infrared (FTIR) spectra were recorded using a HORIBA FT-720 FTIR spectrometer. The morphology of the prepared polymer film was examined by a field emission scanning electron microscope (JEOL 6335F FEG-SEM). Normal incidence optical reflection and transmission spectra were conducted using a high resolution fiber optic UV-visible-near-IR spectrometer (Ocean Optics HR4000). Electrochemical impedance spectroscopy (EIS) was used to study the UV damage effect on the electrochemical behavior of the DSSC with or without UV-shielding polymer film. EIS measurements of DSSCs were carried out using a potentiostat/galvanostat (PGSTAT 30,

Autolab, Eco-Chemie). The frequency range explored was from 0.01 Hz to 1 MHz, using the photo-anode and the Pt-coated ITO glass as working and counter electrode, respectively. The applied bias voltage was set at the open-circuit voltage of the DSSCs. The impedance measurements were carried out under AM1.5 solar radiation. The measurements of the PV performance of the DSSCs were performed using a programmable electrometer equipped with current and voltage sources (Keithley 2400) under solar light illumination (100 mW cm^{-2}) from an AM1.5 solar simulator (Newport Oriel 96000). The measurement of UV-shielding effect was carried out by using 20 W UV bench lamp (Blak-Ray® XX-20BLB) as a light source, and the position of the DSSC from light source is controlled to be 12 cm. The intensity of UV light illuminated on the surface of DSSC is about 1 mW cm^{-2}.

3. Results and discussion

3.1 Morphology and optical properties of UV-shielding polymer film

As shown in Fig. 3(a), the composite consisting of 200 nm silica colloidal crystals exhibited blue color illumined with white light. The high uniformity of the blue color in the photograph was caused by Bragg diffraction of white light from the silica crystalline lattice. Fig. 3(b) displays a cross-sectional scanning electron microscope (SEM) image of the doctor blade coated composite. Although some defects were present, the three-dimensional ordering of 200 nm silica microspheres was observed in the image. It was found that the defects do not significantly affect the optical uniformity of the composite. The long-range hexagonal ordering of silica microspheres was evidenced from the top-view SEM image in Fig. 3(c). Besides, the ETPTA matrix surrounding the silica colloidal crystals was clearly observed in the magnified top-view SEM image in Fig. 3(d).

The embedded 200 nm microspheres in the composite were completely removed by a 2 vol% hydrofluoric acid (HF) aqueous solution wash. The resulting polymer film could be peeled off from the glass substrate easily to create a self-standing macroporous polymer film as seen in Fig. 4(a). The transparent film illumined with white light indicated that incident visible light was not diffracted from the crystalline lattice of 200 nm air cavities. Fig. 4(b) displayed a SEM image of the corresponding templated macroporous ETPTA film. The image revealed the long-range crystalline orderings of 200 nm air cavities, indicating that the macroporous structures did not collapse during the HF-etching procedure. From the magnified top-view and cross-sectional SEM images (Fig. 4(c) and (d)), it was apparent that 200 nm air cavities were interconnected through small windows that resulted from the touching sites of close-packed silica microspheres in the silica colloidal crystal–ETPTA composite. This further demonstrated that the three-dimensional highly ordered 200 nm air cavities were close-packed.

To evaluate the optical properties and the crystalline quality of the doctor blade coated samples, a HR4000 UV-visible spectrometer (Ocean Optics) was used to measure the specular optical reflection and transmission at normal incidence. Fig. 5(a) compared the reflection spectra obtained from a flat ETPTA film, a silica colloidal crystal–ETPTA composite consisting of 200 nm silica microspheres, and a corresponding macroporous ETPTA film. The flat ETPTA film (blue dotted line) exhibited a reflectance of ~10%. Compared with that, the measured reflection peak of the silica colloidal crystal–ETPTA composite (red dashed line) located at 460 nm. The low reflection amplitudes of the peaks resulted from the low refractive index contrast between silica ($n_{silica} = 1.42$) and ETPTA ($n_{ETPTA} = 1.46$). The black solid line displayed the measured reflection peak of the corresponding macroporous ETPTA film spheres located at 360 nm. The high refractive index contrast between

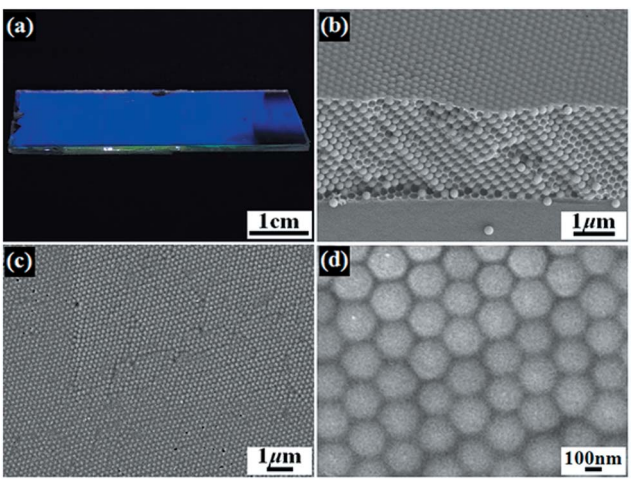

Fig. 3 (a) Photograph of a doctor blade coated silica colloidal crystal–ETPTA composite consisting of 200 nm silica microspheres. (b) Cross-sectional SEM image of the same sample as in (a). (c) Top-view SEM image of the same sample as in (a). (d) Magnified image of (c).

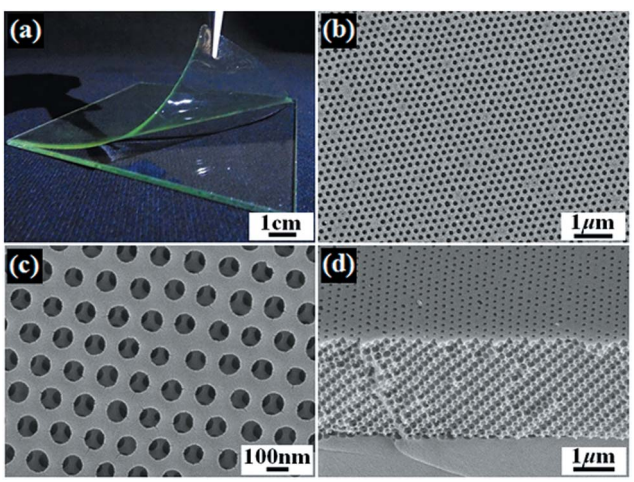

Fig. 4 (a) Photograph of a doctor blade coated macroporous ETPTA film template from 200 nm silica microspheres. (b) Top-view SEM image of the same sample as in (a). (c) Magnified image of (c). (d) Cross-sectional SEM image of the same sample as in (a).

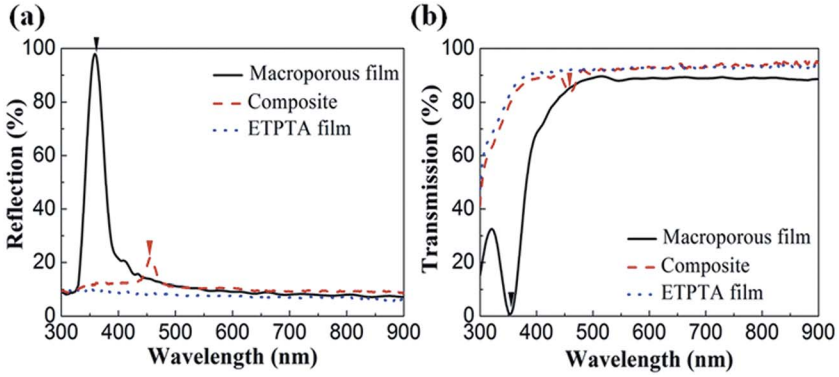

Fig. 5 (a) Normal incidence optical reflection, (b) normal incidence optical transmission spectra obtained from a flat ETPTA film (blue dotted line), a silica colloidal crystal–ETPTA composite consisting of 200 nm silica microspheres (red dashed line), and a corresponding macroporous ETPTA film (black solid line). The arrows indicate the expected positions of the peaks for each sample, calculated using Bragg's law at normal incidence.

air ($n_{air} = 1$) and ETPTA leaded to over 95% reflection of incident ultraviolet radiation. Importantly, the spectrum revealed that the reflection in visible light region was less than 10%, conforming that the macroporous film in Fig. 4(a) was transparent. The positions of the reflection peaks could be theoretically calculated by using Bragg's law:[34]

$$\lambda = 2n_{eff}d \sin \theta \quad (1)$$

where n_{eff} was the effective refractive index of the medium, d was the interlayer spacing, and $\sin \theta = 1$ at normal incidence. It could be noted that the calculated reflection peak positions indicated by the black arrows agreed well with the measured spectrum. This further demonstrated that the doctor blade coated close-packed silica colloidal crystals and the corresponding macroporous films were of highly crystalline qualities. Besides that, normal incidence transmission spectra (Fig. 5(b)) were collected using the same spectrometer. Compared with the flat ETPTA film (blue dotted line), the silica–ETPTA composite showed around 10% lower transmittance at 460 nm, while the macroporous film exhibited less than 3% transmittance in the ultraviolet radiation region and above 85% transmittance for a board band of visible light. This suggested the as-fabricated transparent macroporous film was with excellent anti-UV property.

3.2 Characterization of UV-light illuminated N719 dye anchored TiO_2 and gel electrolyte

To demonstrate the UV-shielding performance of the as-prepared macroporous film on the N719 dye of DSSCs, FTIR spectra of N719 dye adsorbed TiO_2 with or without 2 h UV-light illumination were measured (Fig. 6). For untreated N719 dye, the absorption peaks of thiocyanato group (NCS), carbonyl (C=O), bipyridine (C=C), tetrabutylammonium (TBA) counter-ions, and carboxylic acid and carboxylate groups (C–O) were observed at 2100, 1710, 1542, 1464, and 1256 cm^{-1}, respectively.[35] In addition, the absorption peaks of asymmetric and symmetric vibrations of the COO^- group located at 1624 and 1372 cm^{-1}, respectively.[35] Comparing with the FTIR spectrum of isolated N719 dye, it was clear that the intensity of absorption peaks of N719 dye adsorbed TiO_2 sample were weaker. That was caused by low adsorption content of dye on the TiO_2 nanoparticle surface. Besides, the low intensity of the absorption of NCS group at 2100 cm^{-1} was due to the interaction between the NCS group of N719 dye and TiO_2 surface.[36] Moreover, the absorption peak of COO^- group became broad was attributed to the chemisorbed N719 dye.[37] Apart from that, the FTIR spectra of UV-light illuminated N719 dye adsorbed TiO_2 samples are shown in Fig. 6(c) and (d). FTIR spectrum of the sample coated with an UV-shielding polymer film was not changed significant under UV irradiation. Fig. 6(c) presents the absorption peaks of N719 dye of the sample coated with an UV-shielding polymer film. It was evident that some new absorption peaks appeared for without UV-shielding polymer film coated sample under UV

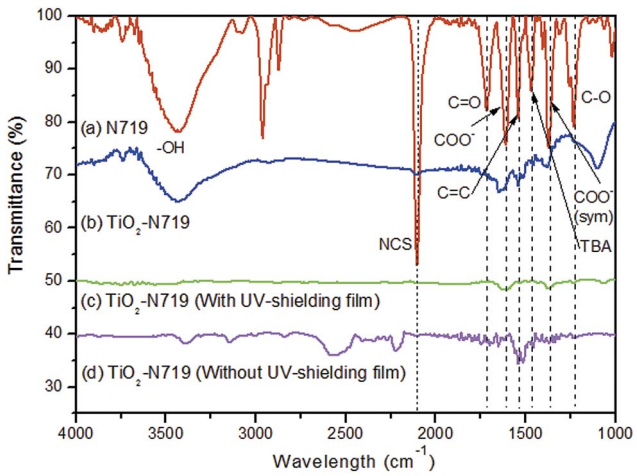

Fig. 6 FTIR spectra of the (a) N719 dye, (b) N719 dye adsorbed TiO_2, (c) UV-light illuminated N719 dye adsorbed TiO_2 (with UV-shielding film), and (d) UV-light illuminated N719 dye adsorbed TiO_2 (without UV-shielding film).

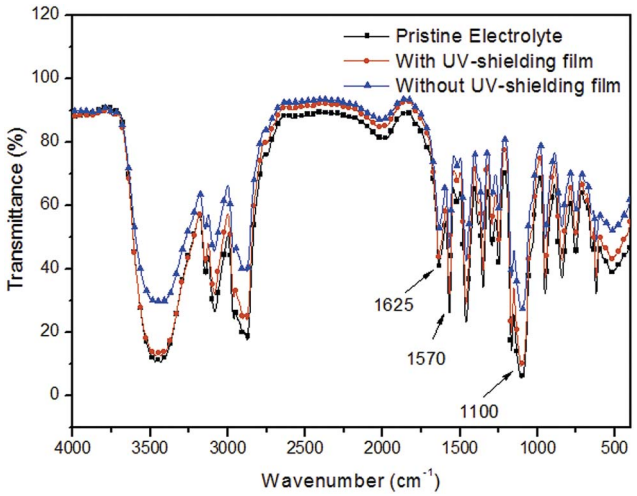

Fig. 7 FTIR spectra of the pristine gel electrolyte, 2 h UV-light illuminated gel electrolyte sample with shielding film, and 2 h UV-light illuminated gel electrolyte sample without shielding film.

irradiation (Fig. 6(d)). This further confirmed that the chemical structure of dye was damaged by UV radiation.

FTIR spectra of the gel electrolyte before and after 2 h UV-light illumination are shown in Fig. 7. The absorption peaks of C–H stretching of alkyl group and ethylene oxide fragment appeared at 2750–3250 cm^{-1}, and the peaks corresponding to C–H stretching of imidazolium ring were observed at 1570 and 1625 cm^{-1}.[38] In addition, the absorption band at 1100 cm^{-1} was attributed to the H–C–C and H–C–N bending of imidazolium groups, and the C–O stretching of ethylene oxide fragment.[38] Furthermore, the intensity of the absorption peaks decreased after UV illumination, especially for the electrolyte sample without UV-shielding polymer film. Nevertheless, the intensity of the absorption peaks of electrolyte with UV-shielding polymer film was slightly decreased as compared to those of the pristine gel electrolyte. This is attributed to the fact of that the UV radiation ranged from 350–400 nm could not be cut by the anti-UV polymer film (Fig. 5(b)).

Table 1 Electrochemical impedance characterization of DSSC with (DSSC I) and without (DSSC II) UV-shielding polymer film (measured under a light intensity of 100 mW cm^{-2} and under the open-circuit voltage)

DSSCs	UV light illumination (min)	R_s (Ω)	R_{ce} (Ω)	R_{rec} (Ω)	R_d (Ω)
DSSC I	0	20.2	22.0	24.6	25.3
DSSC II	0	24.0	18.5	22.5	23.2
DSSC I	120	20.3	24.8	43.5	40.3
DSSC II	120	19.6	132[a]	132[a]	68.5

[a] Sum values (132 Ω) of R_{ce} and R_{rec}.

3.3 UV-shielding effects of macroporous film on the electrochemical impedance of DSSCs

EIS was used to study the UV-damage effect on the electrochemical behavior of the DSSC with or without UV-shielding polymer film coating. Fig. 8 presents the electrochemical impedance properties of DSSCs before and after UV illumination for 2 hours using a Nyquist plot.[39] The equivalent circuit model [inset to Fig. 8] was applied for curve fitting of the electrochemical impendence of DSSCs. The electrochemical impedance properties of the DSSCs before and after UV illumination are summarized in Table 1. In essence, the EIS spectra of an FTO/TiO_2/N719 dye/gel electrolyte/Pt/ITO cell featured three semicircles in the frequency ranged from 10 mHz to 100 kHz. In Fig. 8, the series resistance of the conduction through the working and counter electrodes of the cell was represented by R_s; the capacitance and charge transfer resistance of the reduction of redox species (I_3^- to I^-) at the counter electrode were designated C_{ce} and R_{ce}, respectively; the capacitance and

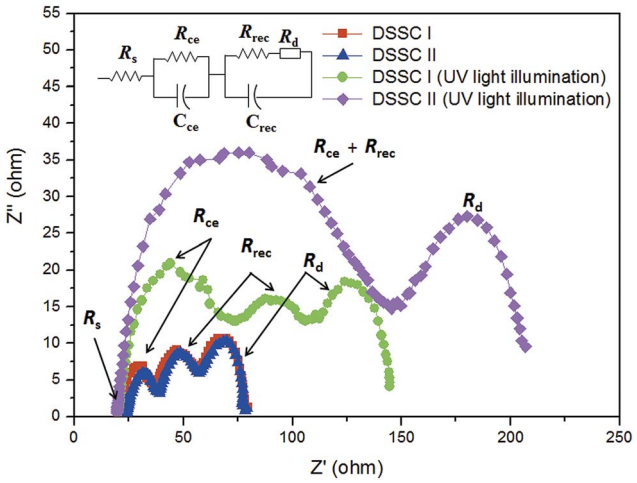

Fig. 8 Nyquist plots of DSSCs before and after 2 h illumination of UV-light; measured under a light intensity of 100 mW cm^{-2} and an open-circuit voltage (inset: equivalent circuit).

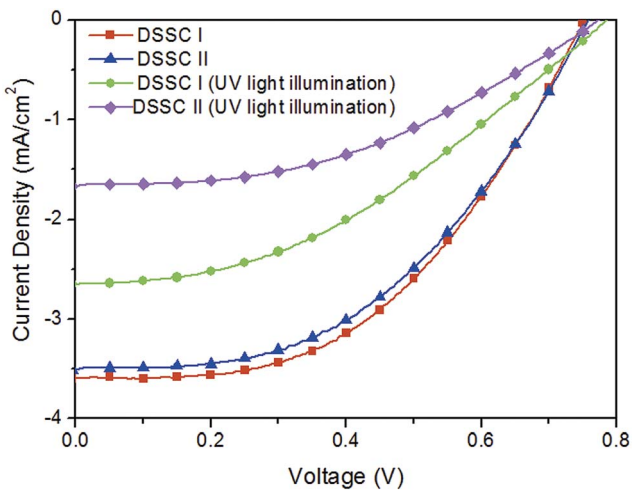

Fig. 9 Current density–voltage plots of DSSCs with (DSSC I) and without (DSSC II) UV-shielding film.

Table 2 PV performance of DSSC with (DSSC I) and without (DSSC II) UV-shielding polymer film

DSSCs	UV light illumination (min)	V_{oc} (V)	J_{sc} (mA cm^{-2})	FF (%)	PCE (%)
DSSC I	0	0.75	18.01	48	6.48
DSSC II	0	0.76	17.45	47	6.23
DSSC I	120	0.78	13.30	43	4.46
DSSC II	120	0.77	8.55	39	2.57

recombination resistance of the charge transfer process between the TiO_2/dye and the electrolyte were represented by C_{rec} and R_{rec}, respectively; and the diffusion resistance or Warburg diffusion process of redox species in the electrolyte was given by R_d.[40,41] The resistances of the DSSCs were obtained by curve-fitting the Nyquist plots with an equivalent circuit model. As shown in Fig. 8, the electrochemical resistances of two DSSCs (DSSC I and DSSC II) without UV illumination were almost the same. The DSSC I had been protected with the macroporous photonic crystal-based UV-shielding polymer film, while the DSSC II had not been protected. After illuminating of UV radiation, the electrochemical resistances were enhanced for both DSSC I and DSSC II. Nevertheless, the enhancement of resistances was much significant for the DSSC II without UV-shielding polymer film coated. Indeed, the UV-shielding polymer film could prevent the damage of UV radiation for the DSSC. The enhancement of resistances for DSSC I and DSSC II was not only the R_{rec}, but also the R_{ce} and R_d. This indicated that the degradation of both N719 dye and electrolyte resulted in the enhancement of the resistances for DSSCs. In addition, the resistances of DSSC I with UV-shielding polymer film were also enhanced after UV illumination. This was attributed to the fact of that the UV radiation ranged from 350–400 nm could not be cut completely by the UV-shielding polymer film.

3.4 UV-shielding effects of macroporous film on the PV performance of DSSCs

Photocurrent density–voltage curves for the DSSC samples before and after 2 h UV illumination are shown in Fig. 9. Table 2 summarized the PV performances of these DSSCs in terms of open circuit voltage (V_{OC}), short-circuit current density (J_{SC}), fill factors (FFs), and PCE. Before the UV illumination, the PV properties of DSSCs with (DSSC I) and without (DSSC II) UV-shielding polymer film were almost the same. For the DSSC II, PV properties were decreased significantly compared to the DSSC I after 2 h UV illumination. The decay of PV performance of DSSC I with UV-shielding polymer film was attributed the

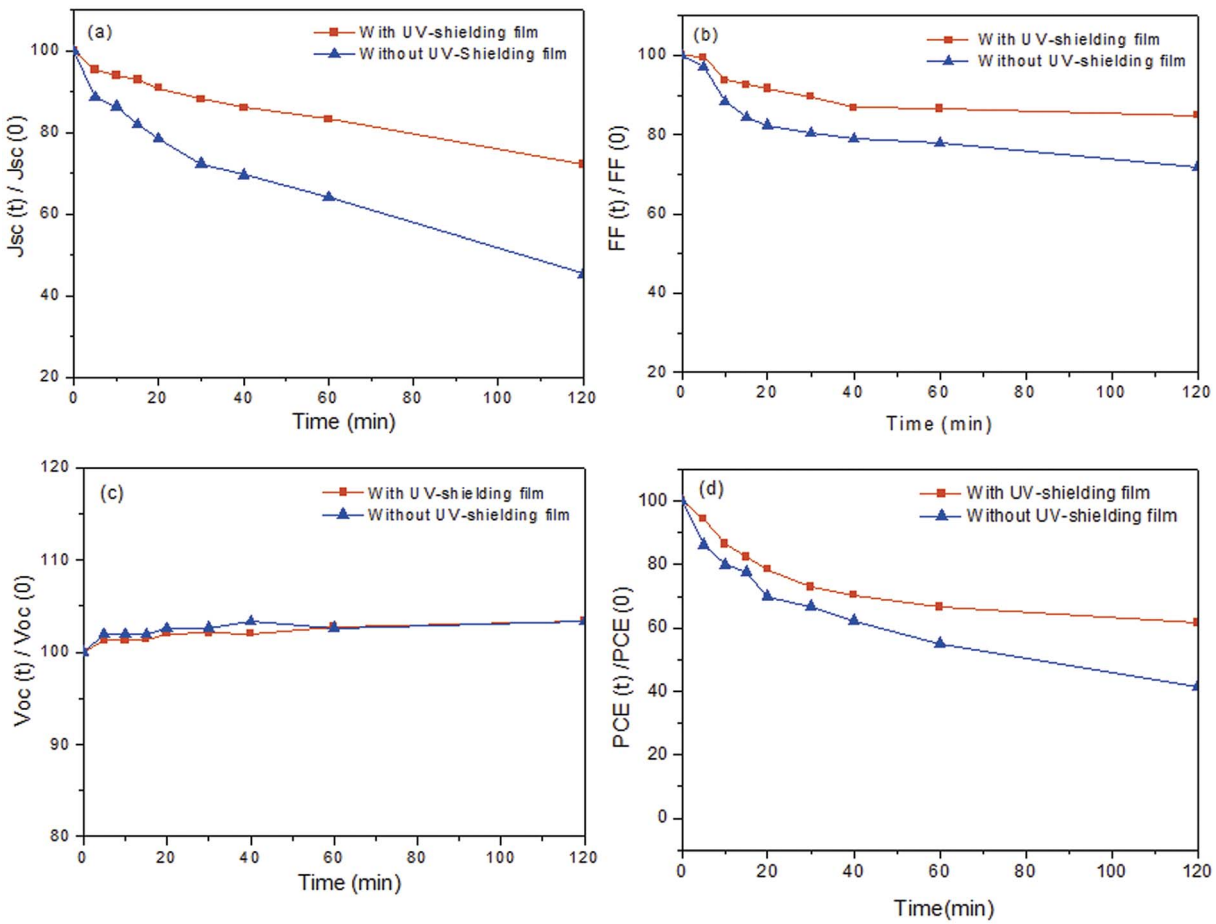

Fig. 10 Stability of PV properties of DSSCs (with and without UV-shielding film) under UV-light illumination.

intrinsic and partially UV degradation of DSSC, while DSSC II was mainly damaged by the UV illumination. The UV degradation of N719 dye and electrolyte resulted in the decrease of PV properties for DSSC II. In addition, the PV stabilities of DSSCs under UV illumination are shown in Fig. 10. The results indicated that the values of J_{SC}, FFs, and PCE of the DSSCs were decreased with the increasing of UV illumination period. The degradation of N719 dye and electrolyte resulted in the increase of the electrochemical resistances of DSSCs. Therefore, the decay of J_{SC}, FFs, and PCE of DSSCs were observed, especially for the DSSC II without UV-shielding polymer film. However, the values of V_{OC} were slightly increased after UV illumination. In essence, V_{OC} was related to the difference between the energy level of the semiconductor electrode and the redox potential of the electrolyte.[42,43] This implied that the energy level of the semiconductor electrode and the redox potential of the electrolyte were affected by the UV illumination.

4. Conclusion

In summary, we had developed a scalable and roll-to-roll compatible colloidal self-assembly technology for fabricating three-dimensional highly ordered macroporous film. The macroporous photonic crystals templated using 200 nm silica microspheres were transparent and could be used directly as the UV-shielding polymer film for N719 dye based DSSC. Comparing with the DSSC coated with UV-shielding film, the enhancement of electrochemical resistances were much more significant for the DSSC without UV-shielding film coating. Besides, PV properties of DSSC without UV-shielding film decreased significantly as compared to that of the DSSC with UV-shielding film. The decay of PV performance of DSSC coated with UV-shielding film was attributed to the intrinsic and partially UV degradation of DSSC, while DSSC without UV-shielding film was mainly damaged by UV radiation. Moreover, the degradation of N719 dye and electrolyte resulted in the seriously decrease of PV properties for DSSC II. This study demonstrated that the efficiency decay of DSSCs was greatly alleviated by the doctor blade coated UV-shielding film.

Acknowledgements

Acknowledgment is made to National Science Council (Grant No. MOST 104-2221-E-005-065-MY3 and 104-2221-E-005-086) for support of this research.

References

1 B. O'Regan and M. Gratzel, *Nature*, 1991, **353**, 737.
2 G. P. Smestad, *Sol. Energy Mater. Sol. Cells*, 1998, **55**, 157.
3 M. K. Nazeeruddin, A. Kay, I. Rodicio, R. H. Baker, E. Muller, P. Liska, N. Vlachopoulos and M. Gratzel, *J. Am. Chem. Soc.*, 1993, **115**, 6382.
4 M. K. Nazeeruddin, P. Pechy, T. Renouard, S. M. Zakeeruddin, R. H. Baker, P. Comte, P. Liska, L. Cevey, E. Costa, V. Shklocer, L. Spiccia, G. B. Beacon, C. A. Bignozzi and M. Gratzel, *J. Am. Chem. Soc.*, 2001, **123**, 1613.
5 Z. Hou, W. Que, J. Ren, Y. Xing, H. M. A. Javed, T. Zhou and L. B. Kong, *Ceram. Int.*, 2015, **41**, S719.
6 Z. Lan, J. H. Wu, J. M. Lin and M. L. Huang, *Sci. China: Chem.*, 2012, **55**, 242.
7 H. G. Agrell, J. Lindgren and A. Hagfeldt, *Sol. Energy*, 2003, **75**, 169.
8 L. C. K. Liau and P. I. Chiang, *Appl. Surf. Sci.*, 2007, **253**, 3982.
9 A. Hinsch, J. M. Kroon, R. Kern, I. Uhlendorf, J. Holzbock, A. Meyer and J. Ferber, *Prog. Photovoltaics*, 2001, **9**, 425.
10 A. Barkschat, T. Moehl, B. Macht and H. Tributsch, *Int. J. Photoenergy*, 2008, 814951.
11 R. H. Lee, T. F. Cheng, J. W. Chang and J. H. Ho, *Colloid Polym. Sci.*, 2011, **289**, 817.
12 Y. C. Hsu, L. C. Tseng and R. H. Lee, *J. Polym. Sci., Part B: Polym. Phys.*, 2014, **52**, 321.
13 B. Macht, M. Turrion, A. Barkschat, P. Salvador, K. Ellmer and H. Tributsch, *Sol. Energy Mater. Sol. Cells*, 2002, **73**, 163.
14 S. Nakajima and R. Katoh, *Chem. Phys. Lett.*, 2015, **619**, 36.
15 K. Tennakone, G. R. R. A. Kumara, I. R. M. Kottegoda and K. G. U. Wijayantha, *Semicond. Sci. Technol.*, 1997, **12**, 128.
16 M. Thomalla and H. Tributsch, *C. R. Chim.*, 2006, **9**, 659.
17 D. Starkey, US 2004/0063840 A1, 2004.
18 T. B. Gorezyca, US 2004/0067366 A1, 2004.
19 S. M. N. Mohsin, M. Z. Hussein, S. H. Sarijo, H. Siti, S. Fakurazi, P. Arulselvan and Y. H. Taufiq-Yap, *J. Biomed. Nanotechnol.*, 2014, **10**, 1490.
20 T. Skowronski, J. F. Rabek and B. Ranby, *Polym. Eng. Sci.*, 1984, **24**, 278.
21 Y. Zhang, S. Zhuang, X. Xu and J. Hu, *Opt. Mater.*, 2013, **36**, 169.
22 S. Li, M. S. Toprak, Y. S. Jo, J. Dobson, D. K. Kim and M. Muhammed, *Adv. Mater.*, 2007, **19**, 4347.
23 P. Vukusic, J. R. Sambles and C. R. Lawrence, *Nature*, 2000, **404**, 457.
24 R. Mayoral, J. Requena, J. S. Moya, C. Lopez, A. Cintas, H. Miguez, F. Meseguer, L. Vazquez, M. Holgado and A. Blanco, *Adv. Mater.*, 1997, **9**, 257.
25 A. Yethiraj and A. van Blaaderen, *Nature*, 2003, **421**, 513.
26 M. G. Han, C. Heo, H. Shim, C. G. Shin, J. W. Kim, Y. W. Jin and S. Lee, *Adv. Opt. Mater.*, 2014, **2**, 535.
27 B. G. Prevo and O. D. Velev, *Langmuir*, 2004, **20**, 2099.
28 S. Zhai, Y. Jiang, H. Zhao and B. Das, *Adv. Opt. Mater.*, 2014, **2**, 632.
29 A. G. Dumanli, G. Kamita, J. Landman, H. van der Kooij, B. J. Glover, J. J. Baumberg, U. Steiner and S. Vignolini, *Adv. Opt. Mater.*, 2014, **2**, 646.
30 H. Jiang, K. Yu and Y. C. Wang, *Opt. Lett.*, 2007, **32**, 575.
31 H. Yang, N. Gozubenli, Y. Fang and P. Jiang, *Langmuir*, 2013, **29**, 7674.
32 W. Stöber, A. Fink and E. Bohn, *J. Colloid Interface Sci.*, 1968, **26**, 62.
33 R. H. Lee, C. H. Chi and Y. C. Hsu, *J. Nanopart. Res.*, 2013, **15**, 1733.
34 P. Jiang, J. F. Bertone, K. S. Hwang and V. L. Colvin, *Chem. Mater.*, 1999, **11**, 2132.

35 F. Hirose, M. Shikaku, Y. Kimura and M. Niwano, *J. Electrochem. Soc.*, 2010, **157**, B1578.
36 J. Singh, A. Gusain, V. Saxena, A. K. Chauhan, P. Veerender, S. P. Koiry, P. Jha, A. Jain, D. K. Aswal and S. K. Gupta, *J. Phys. Chem. C*, 2013, **117**, 21096.
37 F. Hirose, K. Kuribayashi, M. Shikaku, T. Suzuki, Y. Narita, Y. Kimura and M. Niwano, *J. Electrochem. Soc.*, 2009, **156**, B987.
38 T. Rajkumar and G. R. Rao, *J. Chem. Sci.*, 2008, **120**, 587.
39 Y. Zhao, J. Zhai, J. He, X. Chen, L. Chen, L. Zhang, Y. Tian, L. Jiang and D. Zhu, *Chem. Mater.*, 2008, **20**, 6022.
40 Y. C. Hsu, G. L. Chen and R. H. Lee, *J. Polym. Res.*, 2014, **21**, 440.
41 C. H. Chi, Y. C. Hsu, L. C. Tseng, S. Y. Suen, J. Y. Wu and R. H. Lee, *J. Polym. Res.*, 2013, **20**, 269.
42 P. K. Singh, K. I. Kim, N. G. Park and H. W. Rhee, *Macromol. Symp.*, 2007, **249–250**, 162.
43 R. H. Lee, J. K. Liu, J. H. Ho, J. W. Chang, B. T. Liu, H. J. Wang and R. J. Jeng, *Polym. Int.*, 2011, **60**, 483.